Pertanika J. Sci. & Technol. 28 (2): 523 - 544 (2020)

PERTANIKA JOURNALS

SCIENCE & TECHNOLOGY

Journal homepage: http://www.pertanika.upm.edu.my/

Experimental (ADV & PIV) and Numerical (CFD) Comparisons of 3D Flow Pattern around Intact and Damaged Bridge Piers

Ehsan Oveici[1], Omid Tayari[1]* and Navid Jalalkamali[2]

[1]Department of Civil Engineering, Kerman Branch, Islamic Azad University, 7635131167 Imam Ali Blvd., Kerman, Iran
[2]Department of Water Engineering, Kerman Branch, Islamic Azad University, 7635131167 Imam Ali Blvd., Kerman, Iran

ABSTRACT

Numerous bridges fail all over the world every year because of ignoring the role of hydraulic factors, including flow and scour patterns in bridge designs. Hence, investigation of the flow pattern around intact and damaged bridge piers gains significant importance. This study provided experimental and numerical investigations of the flow pattern around damaged and intact bridge piers (short cylindrical and pillar elements). This topic is applicable to flooding conditions of rivers when and where the remainders of bridges and other structures on the river path could affect the flow pattern, making further flow pattern investigations under such conditions necessary. The experiments had been conducted in a straight channel with a length of 12 meters in Kerman, Iran. To collect the three dimensional flow velocity components, Acoustic Doppler Velocimetry (ADV) was employed. Further, Particle Image Velocimetry (PIV) was utilized to compare the results of ADV. SSIIM software helped model the flow in this study, and Navier–Stokes equations and k–ε turbulent model was used for solving the flow field. Generally, the results obtained through the comparisons are indicative of an appropriate correspondence between the numerical and the experimental data. The results indicated that installing the piers along the channel resulted in displacement of the maximum bed shear stress from the last one-third zone of the channel to mid-channel. Also, the maximum bed shear stress increased by 72% in comparison to the case with no piers

ARTICLE INFO

Article history:
Received: 02 December 2019
Accepted: 29 January 2020
Published: 15 April 2020

E-mail addresses:
ehsanoveici@iauk.ac.ir (Ehsan Oveici)
tayari@iauk.ac.ir (Omid Tayari)
njalalkamali@iauk.ac.ir (Navid Jalalkamali)
* Corresponding author

ISSN: 0128-7680
e-ISSN: 2231-8526

installed. Moreover, the maximum water level variations occurred in the case with both intact and damaged piers installed, where there was water level reduction downstream and water level increase upstream of the pier.

Keywords: 3D flow velocity, acoustic Doppler velocimetry, bed shear stress, bridge piers, experimental model, particle image velocimetry, SSIIM

INTRODUCTION

Statistics have shown a significant increase in the number of damaged bridges as time passes. This difference may to some extent be attributed to statistical flaws in past years or the increase in the number of bridge constructions; however, Melville and Coleman (2000) believed that not only were new scientific rules ignored in construction of bridges in recent years, but inaccessibility of the practical results of research on scour to those active in this field and eventually the current status of our knowledge on scour and bridge hydraulics also counted as the main reasons for the increase in the number of instances of such damage. The extremely important issue of bridge failure has had numerous scientists seeking to know as much as possible about scouring phenomena and complex flow patterns. They have tried to predict behavior under varied circumstances by resorting to different methods, including incorporation of physical, numerical and field research models. A number of these will be cited in the following:

Chiew and Melville (1987) studied the effect of flow velocity, flow depth, and sediment particle size on the scour depth around cylindrical piers. They found that where the flow velocity was higher than the incipient motion value, increasing the flow velocity by up to twice the incipient motion value reduced the scour depth to a minimum value. Breusers and Raudkivi (1991) examined the scour around piers by altering cross-sections. They concluded that the pier with increased cross-section upward (towards the water surface) increased the scour, and the pier with decreased cross-section upward reduced the scour. Bozkus and Yildiz (2001) studied the effect of a single pier inclination, and Bozkus and Cesme (2010) addressed the effect of dual bridge piers on scour depth in a straight channel. They reported a reduction of scour depth by increasing the pier's angle in the downstream direction. Vaghefi et al. (2016b) studied and compared flow patterns and local scour around inclined and vertical cylindrical piers under clear water conditions. They investigated the effect of pier inclination in three directions: upstream, downstream, and perpendicular to the flow. They demonstrated that for every degree of increase in pier inclination, the scour depth was reduced by about 1% in comparison to a vertical pier position. Khajeh et al. (2017) undertook an experimental study and comparison of scour depth and position around an inclined cylindrical pier and a vertical pier at a 180-degree sharp bend apex. They concluded that installation of the pier towards the outer bank had created alternating sedimentary dunes at the downstream side of the pier in the vicinity of the inner bank. Jaman et al. (2017) carried out an experimental study of scour around three identical

circular-type piers arranged inline and eccentrically in a staggered manner. Two inline piers were positioned towards the flow, and the eccentric one was placed in the middle region of the two inline piers. They found that vortices' strengths for the eccentric-middle and inline-rear piers were the greatest and the lowest, respectively, compared with strength of the inline-front pier. Karimi et al. (2017) studied the effect of bridge pier inclination angle on the scouring process under clear water conditions in a straight channel. Results of their study indicated that the minimum and the maximum scour depths occurred from 0 to 15-degree angles. Vaghefi et al. (2018b) examined scour around a triad series of piers, perpendicular to or in the direction of the flow, under clear water conditions in a laboratory flume with a width of 100 cm and a 180-degree sharp bend. As the results of their study indicated, with installation of the piers in perpendicular and streamwise directions, the maximum scour hole occurred at the 60-degree angle, around the piers, with sedimentary dunes observed at the downstream side of the piers. Bozkus et al. (2018) examined the effects of inclination of upstream and downstream piers in triad and quad pier groups on scouring. To this aim, they conducted tests for two different cases involving three and four piers either in a perpendicular position or with inclination angles of 10 and 15 degrees, with two diameters of 50 and 70 mm under clear water and steady-state sediment conditions. Totally, they ran 72 tests and concluded that increasing the pier diameter and the flow rate increased the scour. Omara et al. (2018) incorporated Flow-3D model in order to obtain the water surface, flow velocity, bed shear stress, and scour depth around vertical and inclined piers. They also compared these with experimental data and demonstrated that the Flow-3D model could efficiently model the depth of the free surface water and the velocity of the flow with a high accuracy. Asadollahi et al. (2019) carried out numerical and experimental comparison of the flow and scour patterns around single and triad piers which were installed in a 180-degree sharp bend. Results of their comparisons suggested the appropriate calculations of the numerical data and the great competency of SSIIM in modeling the flow and scour patterns with a maximum error of only 4% reported for the scour and sedimentation.

As noted, most research efforts attempted to date to investigate bridge piers in rivers concern the scour phenomenon and study of its mechanism and the maximum values around conventional piers (Breusers & Raudkivi, 1991; Bozkus & Yildiz, 2001; Bozkus & Cesme, 2010; Khajeh et al., 2017; Jaman et al., 2017; Karimi et al., 2017; Vaghefi et al., 2018b; Bozkus et al., 2018). Few researchers have ever addressed the complex flow pattern around intact and damaged bridge piers. Firstly, 3D analysis of the complex flow pattern around intact and damaged bridge piers requires great hydrodynamic knowledge and sufficient proficiency on this topic. Secondly, the laboratory equipment required for this research (ADV and PIV velocimeters) are barely accessible to researchers due to their great cost. Therefore, this study investigated the flow pattern in a straight channel under the influence of a single intact pier, a single damaged pier, and the effect of both piers

with an experimental method (by using two different velocimeters: ADV and PIV) and a numerical method (by using CFD model). Application and significance of this point were further experienced under flooding conditions of rivers, for the wreckage of the bridges and other structures were present on river paths and could influence the flow pattern. The need to investigate the flow pattern is more evident under such conditions. In addition, although the bed of this channel is rigid, calculation of bed shear stress in this study allows estimation of the scour phenomenon under mobile bed conditions as well.

MATERIALS AND METHODS

Introduction of the Experimental Model

Laboratory Channel. To conduct the intended study, a 1-meter-wide, 0.8-meter-high laboratory channel with glass walls and steel frames was designed and constructed in the laboratory of hydraulic structures at Islamic view of the channel in the laboratory. As seen in Figure 1, the channel's effective length is 12 meters. The laboratory channel bed is rigid

(a)

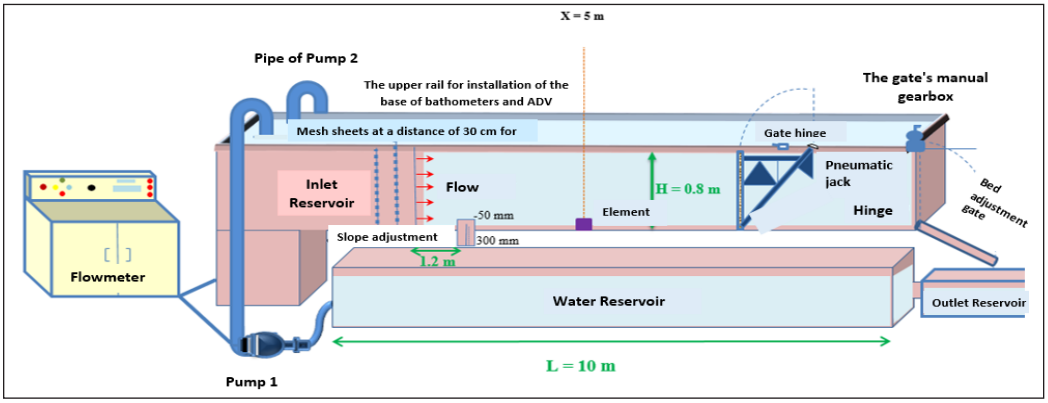

(b)

Figure 1. (a) A view of the channel in the laboratory; and (b) a schematic view with the components of the channel in the laboratory of the hydraulic structures at Islamic Azad University, Kerman Branch

and is made of steel. Side reservoirs with an approximate capacity of 10 m^3 have been used as sources of water in this channel. Two H25-200 centrifugal pumps, with a snail-shaped scroll made by Pumpiran Co. pump water from the reservoirs were embedded at the side of the channel into the channel's inlet reservoir. The discharge capacity of 60 liters per second was kept constant throughout every experiment by using an AKTEK ultrasonic flow meter with ±1 mm/s accuracy. Water had been pumped into the inlet reservoir with this discharge capacity by the pumps. These pumps are linear, and each is capable of generating a maximum 190 m^3/s discharge. Further, the water level at the upstream is 20 cm, the depth which was set by using the butterfly gate at the end of the downstream path for conducting the experiments, because the ratio of width to depth of the flow must be equal to or greater than 5 or 6 in order to reduce the effect of the channel sidewalls according to Nezu and Nakagawa (1993). To calm the inlet flow and to reduce the initial turbulence during the experiments, two mesh sheets were also embedded at the inlet reservoir connection 25 cm apart from each other.

Bridge Piers. Elements used in conducting the experiments include a short cylindrical element (with a diameter of 10 cm and a height of 5 cm), and a column element (with a diameter of 4 cm and a height of 40 cm), where the short cylindrical element represents the damaged bridge piers or flood debris present on the flow path, and the column element represents a bridge pier in river. The cylindrical element is made of solid steel, and the column is hollow PVC pipe with 3-mm-thick walls with a powerful magnet installed at the end to make it adhere to the channel bed. The height of these elements had been determined according to recommendations of Yeow et al. (2016). Furthermore, these two values had been specified for determination of the element's diameters according to research results:

1. According to observations by Chiew and Melville (1996), the bed element's diameter must be smaller than or equal to 10% of the channel width to remove the effect of channel sidewalls on the flow pattern.
2. According to Raudkivi and Ettema (1983) standard, the channel width must be at least 6.25 times the pier diameter.

These elements were located at mid-channel at a distance of 5 meters from upstream.

ADV and Relevant Software Programs. Vectrino 3D velocimeter, which is one of the most advanced ADV's (Acoustic Doppler Velocimetry), had been utilized to measure velocity components and determine the 3D flow pattern. The device function involves sending a sound wave with a specific frequency and receiving its reflection from the flow to identify the flow velocity from the extent of variations in the initial frequency. This device has two side-looking and down-looking probes based on the position of its sensor to be used to measure different sections of the field (Nortek, 2009). To carry out the experiment, a frequency of

25 Hz and a time of 1 minute were assumed (Vaghefi & Akbari, 2019). Hence, the device is capable of collecting the flow velocity in three directions up to 1500 data per minute. During the experiments, it has always been considered to keep the values of "Coloration" and "Signal to Noise Ratio" above their standard values (respectively 80 and 20%) in order to increase the accuracy of the velocimeter's measurements. The information on the data measured at different times was recorded by Vectrino and saved as ADV format. Then these data were converted into vno format in order to be used in Explorer V for filtration. They were then converted into a format usable in Excel after analysis and velocity averaging (Akbari & Vaghefi, 2017). Figure 2 illustrates a view of data collection by ADV around intact and damaged bridge piers.

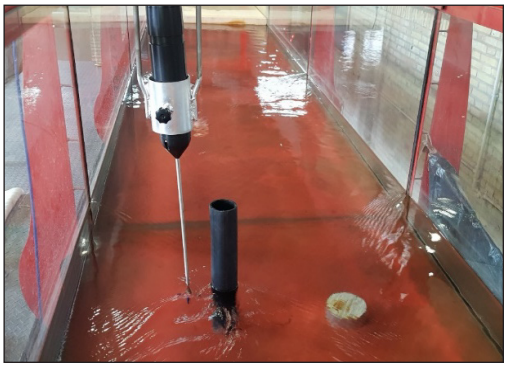

Figure 2. Position of ADV for data collection around the two elements present in the channel

Particle Image Velocimetry (PIV). PIV had been utilized along with a down-looking probe of ADV to measure the flow velocity throughout these experiments. The main advantage of this velocimeter to ADV was the fact that it did not cause local turbulence and streamline variations caused by the presence of probes on the flow path in measurements, and hence increasing the accuracy of data measurement (Rusello et al., 2006; Hurther & Lemmin, 2001; Voulgaris & Trowbridge, 1998). Furthermore, since velocity data were collected at points and at very close intervals, PIV was the best choice for monitoring velocity variations around the hydraulic structures, the vicinity of the water surface, and the walls, especially in turbulent flows. Figure 3 depicts the flow velocity measurement by using PIV. According to this figure, when collecting the flow velocity by using PIV, the laser source is installed on top of the flume by using a mobile platform in such a way as to create a rectangular plane. This plane, as wide as the flow depth, has a streamwise alignment (the length of which depends on the distance of the laser), and is two dimensional. Then the camera was installed on a tripod with an adjustable height at a distance of 91 cm from the outer wall of the flume. After the connections between the laser, the camera, and the data collection and the recording system (a computer equipped with a special card) were constructed with a switch, eventually, the data collection and recording operation was undertaken by running the velocity data recording software (rtcontrol) (Thielicke & Stamhuis, 2014). Also, PIVLab software has been utilized for processing and analyzing the output images (Raffel et al., 2018).

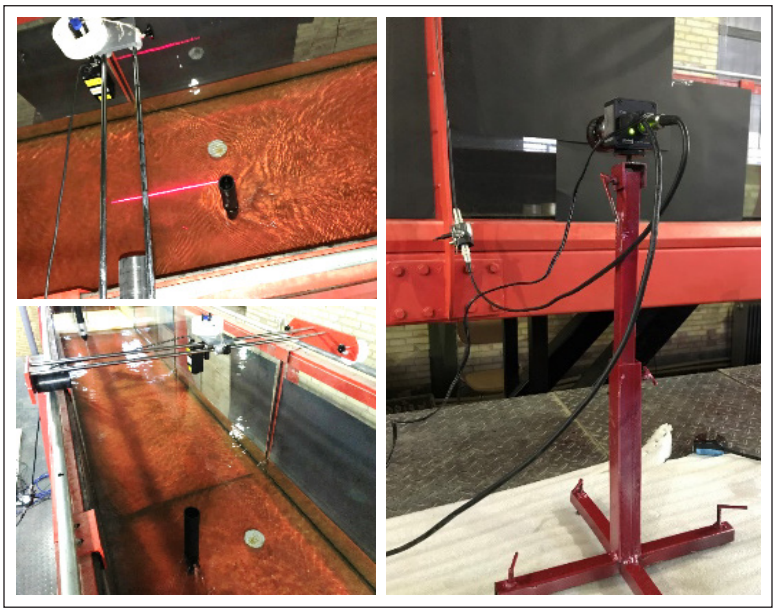

Figure 3. A view of the flow velocity measurement by using PIV and the relevant equipment

The Number of Data Collection and Experiments. A finer mesh was generally used throughout the experiment in the area of the elements and their downstream side. For instance, Figure 4 illustrates the grid network for the experiment with no piers present. In this figure, Z denotes the water depth at the channel's entrance, Y represents the channel width, L is the channel length, and H is the channel height. However, considering the higher sensitivity of the experiments involving piers and the need for more accuracy, finer meshes had been used so that the 3D velocity profile occurred in 13 cross-sections along

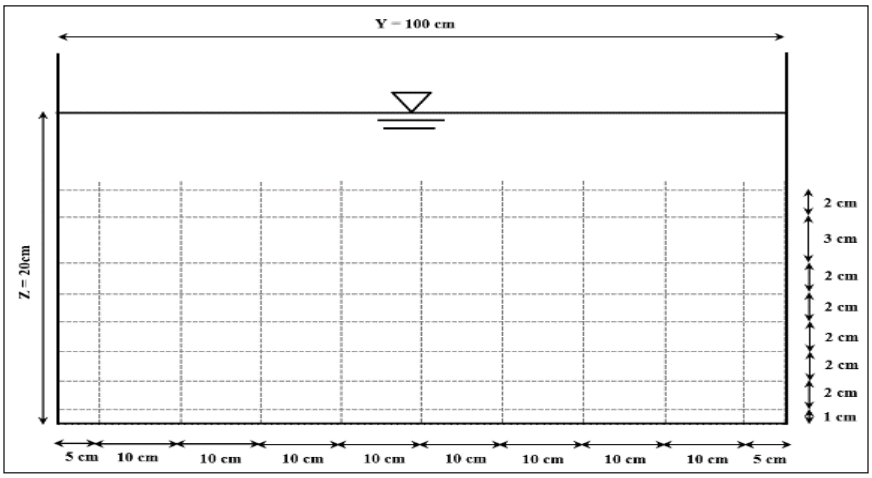

Figure 4. Channel transverse grid for determining the position of the collected points in the experiment with no piers present (the figure has no scales)

the channel and 7 levels of depth, and 20 points were collected in every transverse axis. Considering the aims of this study, the number and order of the specified experiments are presented in Table 1.

Table 1
The number and order of flow pattern experiments

Experiment No.	Experiment Name	Structure Type (Channel Bed Conditions)
1	Test 1	Bed without piers
2	Test 2	Bed with a damaged pier
3	Test 3	Bed with an intact pier
4	Test 4	Bed with both piers

Numerical Model

SSIIM Software. SSIIM (Sediment Simulation in Intakes with Multiblock option) is considered as one of the best CFD software programs. It is used for numerical analysis of scour and flow patterns in channels and rivers and generally the issues about river engineering and hydraulics. This software solves Navier-Stokes equations with the standard K-ε turbulence model on a 3D network. The Finite Volume Method had also been used with the power algorithm and the second-order directional algorithm for discretization. Further, the SIMPLE method was used for the relationship between the pressure and the velocity terms. By using an implicit solution, the velocity field was calculated in the geometry, and by using the calculated velocity field and solving the continuity equation of the sediment, the bed variations were calculated.

Governing Equations of Flow. The Navier-Stokes equations are the equations governing the flow in this software, and the turbulence model is used for solving them. SSIIM numerical model is capable of employing different turbulence models. After considering the previous studies conducted by other researchers (Vaghefi et al., 2016c; Vaghefi et al., 2017) and different turbulence models, the K-ε model was selected as the turbulence model. Navier-Stokes equations for incompressible fluids with a constant density in a vector are as follows (Equation 1):

$$\frac{\partial U_i}{\partial t} + U_j \frac{\partial U_i}{\partial x_i} = \frac{1}{\rho} \frac{\partial}{\partial x_i} \left(- P\delta_{ij} - \rho \overline{u_i u_j} \right) \quad (1)$$

where

x_1, x_2, and x_3 are distances in three directions; U_1, U_2, and U_3 denote velocity in three directions; P is the total pressure; and δ_{ij} is Kronecker delta, which is unity if i=j, and null otherwise.

The first term on the left in the above equation is the transient term (temporal variations), and the next term is the displacement term. The first term on the right is the pressure term, and the next term pertains to the Reynolds stress. Evaluation of the latter requires a turbulence model. Boussinesq proposed Equation 2 to state the Reynolds stress term for k-ε turbulence stress:

$$-\overline{u_i u_j} = \nu_T \left(\frac{\partial U_j}{\partial x_i} + \frac{\partial U_i}{\partial x_j} \right) + \frac{2}{3} k \delta_{ij} \tag{2}$$

$$\nu_T = c_\mu \frac{k}{\varepsilon^2} \tag{3}$$

k (the flow kinetic energy), P_k, and ε (the kinetic energy loss) are modeled as Equations 4 - 6:

$$\frac{\partial k}{\partial t} + U_j \frac{\partial k}{\partial x_j} = \frac{\partial}{\partial x_j} \left(\frac{\nu_T}{\sigma_k} \frac{\partial k}{\partial x_j} \right) + P_k - \varepsilon \tag{4}$$

$$P_k = \nu_T \frac{\partial U_j}{\partial x_i} \left(\frac{\partial U_j}{\partial x_i} + \frac{\partial U_i}{\partial x_j} \right) \tag{5}$$

$$\frac{\partial \varepsilon}{\partial t} + U_j \frac{\partial \varepsilon}{\partial x_j} = \frac{\partial}{\partial x_j} \left(\frac{\nu_T}{\sigma_\varepsilon} \frac{\partial \varepsilon}{\partial x_j} \right) + C_{\delta 1} \frac{\varepsilon}{\kappa} P_\kappa + C_{\delta 2} \frac{\varepsilon^2}{\kappa} \tag{6}$$

In the k-ε turbulence model in the above equations, the constant values are as follows:

$$c_\mu = 0.09 \qquad C_{\varepsilon 1} = 1.44 \qquad C_{\varepsilon 2} = 1.92 \qquad \sigma_\kappa = 1.0 \qquad \sigma_\varepsilon = 1.3$$

Water Surface Profile. The free surface was computed using a fixed-lid approach with zero gradients for all variables. The location of the fixed lid and its movement as a function of time and the water flow field were computed by pressure and the Bernoulli algorithm: It uses the Bernoulli equation along the water surface to compute the water surface location based on one fixed point that does not move. Considering two consecutive cross-sections "j" and "j+1", we can use the extended Bernoulli equation to write Equation 7:

$$W_{j+1} + a_{j+1} . V_{j+1}^2 / 2g = W_j + a_j . V_j^2 / 2g + h_r \tag{7}$$

where W_j denotes the water surface elevation above water level (or a reference surface), V_j is the average velocity in a cross-section, the coefficient α_j is equal to unity, and h_r is the friction loss due to the influence of roughness (Equation 8):

$$h_r = J_e . \Delta x \quad (8)$$

where Je denotes the energy gradient and Δx is the horizontal distance between cross sections "j" and " j+1". The energy gradient Je can be quantified by making use of the Gauckler-Manning-Strickler equation to yield Equation 9:

$$J_e = 1/(k_{st}^2 . R_{h.m}^{4/3}) . V_m^2 \quad (9)$$

where k_{St} is the Strickler coefficient, and V_m and $R_{h,m}$ are the mean average velocity and the mean hydraulic radius of the two consecutive cross-sections (Vaghefi et al., 2016c).

Grid System. The sizes of mesh near the bridge piers were smaller than those upstream and downstream of the piers so that better results might be achieved. A structured grid was used in SSIIM-1 (Olsen, 2003). Figure 5 illustrates the mesh grid considered for longitudinal and cross sections, and in fact the computational domain intended for this study. With the aim of sensitivity analysis for the mesh grid of the model, three different grids (fine, medium, and coarse) were used with respective dimensions of 3067894, 1073226, and 500769. Based on these mesh grids, the best model had been analyzed on the number of cells and efficiency. Table 2 provides the values of the comparison of the numerical model with the experimental results for the case without piers. Comparisons presented in this table are given for the longitudinal velocity at a distance of 4 meters from the channel upstreamside. In this table, R^2 is the coefficient of determination and RMSE stands for Root Mean Square Error. According to this table, it may be observed that the appropriate mesh grid of the numerical model with the most similar results to the experimental model has 1073226 cells. Moreover, the appropriate time required for the software to carry out computations for the finer mesh has been several times greater than that required for the average mesh. Therefore, the average mesh has the most efficiency and the best evaluation

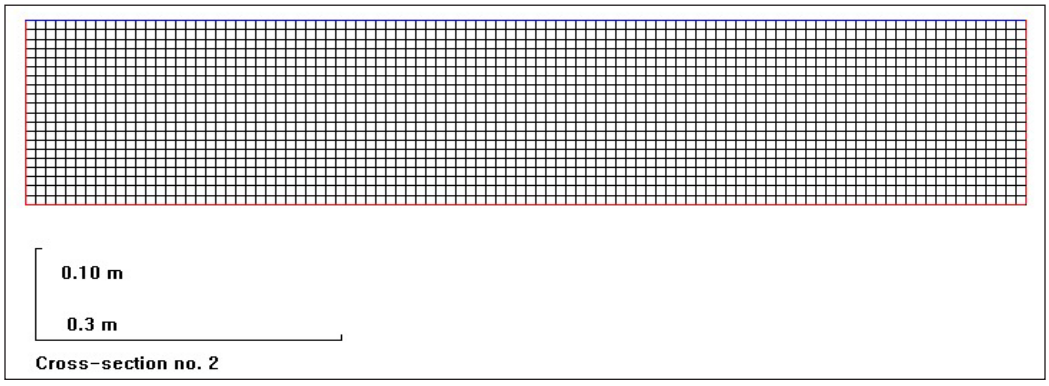

Figure 5. An illustration of the mesh grid and the computational domain considered for longitudinal and cross sections

and has been selected as the optimum mesh for numerical modeling. The grid systems in the vertical, lateral and longitudinal directions (stream wise) respectively have 21, 101, and 506 lines, and in total they have 1073226 cells.

Table 2
The results of evaluating the efficiency of the cells' size and sensitivity analysis of the mesh for the longitudinal velocity at a distance of 4 meters upstream

Mesh Size	R^2	RMSE
Coarse mesh	0.9383	0.0195
Medium mesh	0.9823	0.0107
Fine mesh	0.9771	0.0478

Boundary Conditions. The discharge value must be defined as the input boundary condition. The gradient of all the parameters at the output boundary equals zero. Besides, the discharge at the downstream side must also be defined as the output boundary condition. The ε gradient (the kinetic energy loss) and also the value of k (the kinetic energy) are assumed to be zero at the water surface. The flux passing through the bed and wall is null, and the law of the wall proposed by Schlichting (1979) is used as in Equation (10), where U is velocity, U* denotes shear velocity, K represents a constant coefficient equal to 0.4, y is the distance of the wall from the center of the cell, and Ks is roughness equal to d_{90} in the soil gradation curve (Olsen, 1999; Olsen, 2001; Olsen, 2003):

$$\frac{U}{U*} = \frac{1}{K} \mathrm{Ln}(30y/K_s) \qquad (10)$$

The analysis was made under clear water conditions, for the maximum scour depth occurs under such conditions (assuming a non-rigid bed). The input discharge at the upstream side of the channel equaled 60 liters per second. The water depth and the Froude number at the channel's entrance were 20 cm and 0.34, respectively. Also, the channel walls and the bed had been assumed rigid.

Initial Conditions. The input discharge at the upstream side of the channel equaled 60 liters per second. The water depth and the Froude number at the channel's entrance were 20 cm and 0.34, respectively. Also, the channel walls and the bed had been assumed rigid.

RESULTS AND DISCUSSION

The open-channel flow has a thoroughly three-dimensional structure and is turbulent due to the dominant boundary conditions (the input flow intensity as well as bed and wall conditions). It is naturally vital to gain sufficient knowledge of hydrodynamic phenomena in open-channel flows with no obstacles before investigation of complex flow patterns and

the structure of turbulent flows resulting from construction of intact and damaged bridge piers. Hence, in every section related to the results of this study, every parameter calculated and analyzed in four cases, without the piers, with a damaged pier, with an intact pier, and with both intact and damaged piers, has been provided following these results.

Verification

First, to validate the results obtained from the numerical model made by SSIIM software, they were compared and validated with the experimental results collected by using ADV under the same conditions. Figure 6 depicts experimental and numerical results of longitudinal velocity components at a cross-section at a distance of 5 m from the upstream side of the channel and at mid-channel in four cases (without piers, with a damaged pier, with an intact pier, and with both intact and damaged piers). As is observed in these figures, in every case, the flow velocity is the minimum near the bed but increases towards the water surface where the boundary layer fades. It may be observed in Figure 6 that the highest difference between numerical and experimental data is at the layers near the bed. This has also been reported in studies of other researchers who have compared ADV collected data with those of CFD software programs (Vaghefi et al., 2016c; Vaghefi et al., 2019c; Asadollahi et al., 2019).

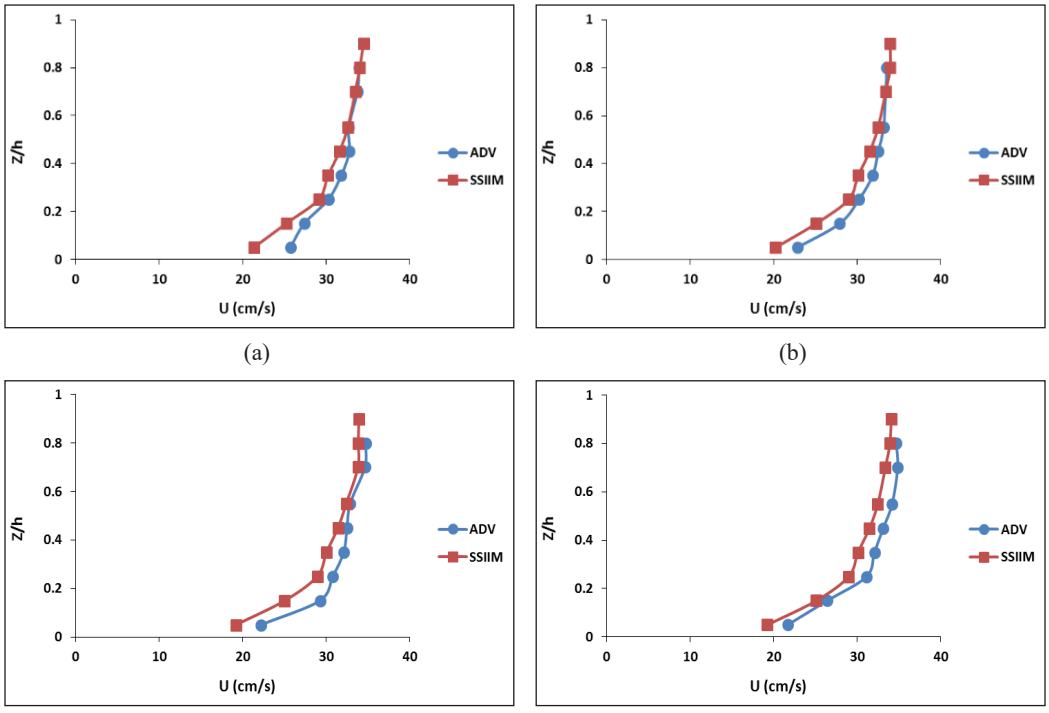

Figure 6. Comparison of numerical and experimental data for a) Test 1, b) Test 2, c) Test 3, and d) Test 4

In every case presented in Figure 6, ADV has provided higher values than SSIIM output data. Moreover, in Test 1, there is less flow turbulence due to the absence of structures on the flow path, and there is a higher correspondence observed between numerical and experimental data. Lack of a total correspondence between numerical and experimental results in other cases is due to the difference in the nature of the numerical and experimental studies. On the other hand, the high sensitivity present in the experimental research due to the difficulty of data collection in sensitive areas such as the vicinity of the pier and also the contacts between the velocimeter probes and the pier could reduce the accuracy of the collected data and lead to differences between numerical and experimental results. Also, simplifications made in solving the equations through numerical calculations contribute another factor reducing the complete validity of the numerical results. Nevertheless, the average error present in every case is less than 5% and it indicates similarity of the results obtained through SSIIM software and the experimental results, which is, in fact, indicative of data analysis validity.

Comparison between ADV and PIV Data

Figure 7 presents longitudinal velocity components at a cross-section at a distance of 5 m from the upstream sections and at mid-channel for all four cases to compare PIV and ADV data. As is clear in the figure, PIV data enjoy a higher unity and number because they are collected in-depth and at a specific level. This entails a clearer observation of flow variations and higher accuracy in measurements; it is not possible to collect data up to the vicinity of the water surface by ADV because the data are collected at a distance of 5 cm from the probe. As is observed in Figure 7, the values collected by ADV are higher than PIV velocity values. Furthermore, again, the difference in these data is evident in the values collected near the bed, the issue previously reported by other researchers comparing ADV and PIV data (Kara et al., 2012; Tominaga & Nezu, 1991; Nabipour et al., 2018).

As previously stated, the main advantage of PIV over ADV is the fact that no local turbulence and streamline variations occur due to the absence of probes on the flow path when measuring velocity, and the accuracy of data measurement is enhanced. Recent years have seen numerous studies conducted on 3D velocity components collected using ADV by researchers including Goring and Nikora (2002), Shinneeb et al. (2004), Westerweel and Scarano (2005), Mori et al. (2007), Duncan et al. (2011), Razaz and Kawanisi (2011), Razaz et al. (2013), Islam and Zhu (2013), Yafei (2015), Vaghefi et al. (2017), Vaghefi et al. (2019a), and Vaghefi et al. (2019b). There have been studies addressing spike data, and proposing an algorithm for removing such data, and they have also proved the presence of data inconsistent with the pattern of other data. Nevertheless, the difference between the average flow longitudinal velocity data for the conducted experiments has been approximately 4% (3.9%), which is negligible, for the same 4% error has also been

reported in previous studies (Lemmin & Rolland, 1997); whereas, the error is much bigger in transverse and vertical velocity components as well as in turbulence components (Kara et al., 2012; Tominaga & Nezu, 1991).

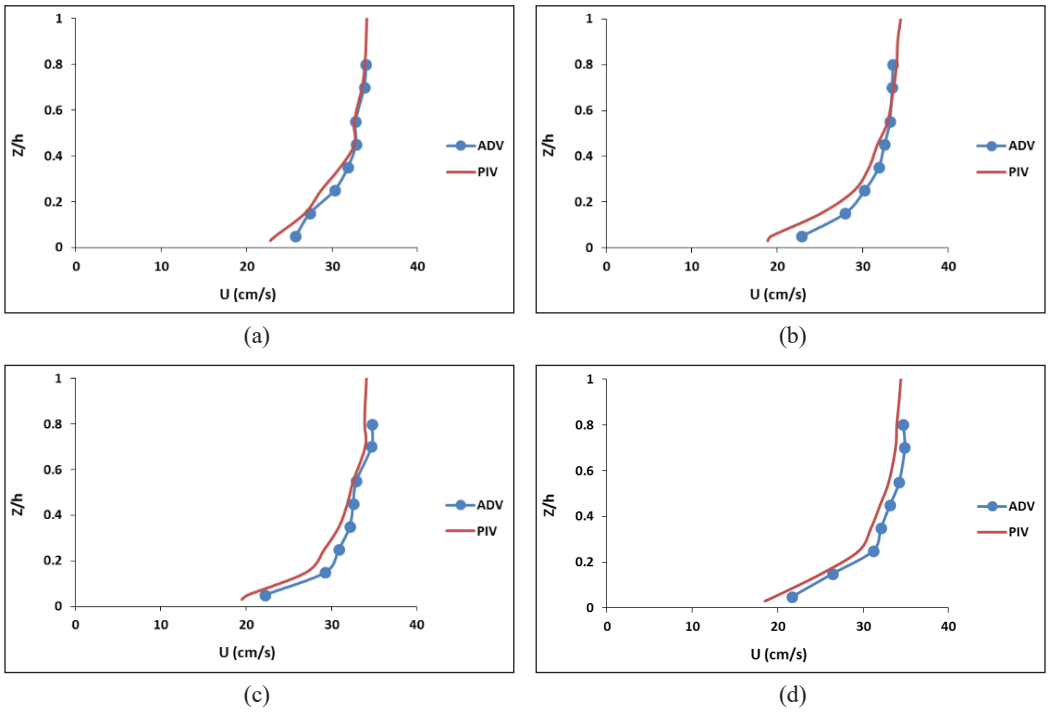

Figure 7. Comparison of ADV and PIV experimental data in a) Test 1, b) Test 2, c) Test 3, and d) Test 4

Streamlines

This section investigates streamlines at the cross section and longitudinal section, and plans to study the flow pattern under the influence of intact and damaged piers in a channel with or without piers.

Streamlines at Cross Sections. Figure 8 depicts an instance of streamlines at a cross-section at a distance of 5 m from the upstream side of the channel in four different cases. As is seen in this figure, the effect of present damaged and intact piers on flow pattern variations in the river path is evident, for the streamlines create return flows after colliding with the intact pier; whereas, in the case of the damaged pier, the flow passes over the pier due to its submergence. The combined effect of damaged and intact piers creates downflow streams in the area of the piers, the fact which has resulted in bed shear stress increase; therefore, assuming mobile bed conditions, it causes scour in the vicinity of the bridge piers. Presence of these downflow streams has also been reported in the studies of other researchers including Vaghefi et al. (2018a), where they employed protective structures

along with spur dikes, as well as the research where they additionally used submerged, short spur dikes (Vaghefi et al., 2016a). Further, a tranquil and semi-stagnant area has been formed between the two piers due to the creation of low-velocity streams. This phenomenon occurs under the influence of the intact pier located near the inner wall of the channel as an obstacle to high-velocity streams.

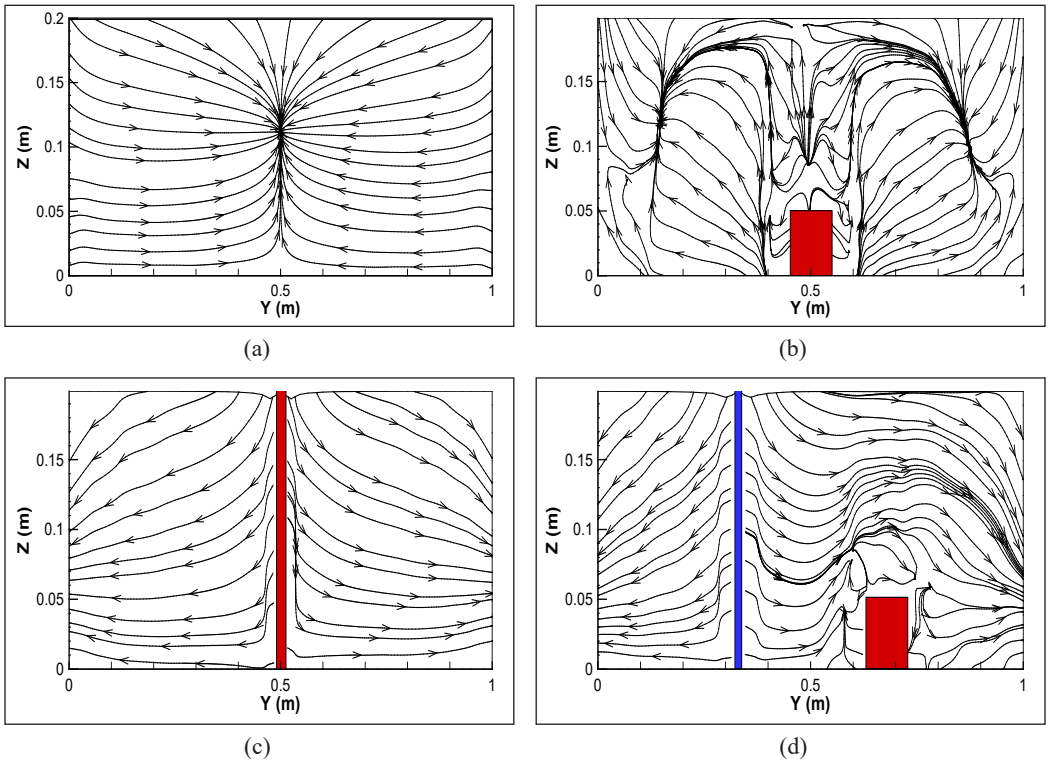

Figure 8. An instance of streamlines at cross-section at a distance of 5 m upstream in a) Test 1, b) Test 2, c) Test 3, and d) Test 4

Streamlines at Longitudinal Sections. To study the streamlines at longitudinal sections, Figure 9 illustrates the results of analysis of these streamlines at mid-channel in four different cases. As is observed, when there are no structures on the flow path, the streamlines have stretched along the path; whereas, with the installation of the 5 cm-high damaged pier, the streamlines at this area shift path into upflow after collision with the pier, and then appear downflow after passing over the pier. Downflow streamlines indicate the destructive streamlines and suggest the possibility of scour at the downstream side of the pier (Vaghefi et al., 2016c); therefore, the flow velocity is expected to decrease in this area. However, it is different for the intact pier because it is not submerged, and the downflow streamlines have appeared at the upstream side of this intact pier. The effects entailing creation of upflow and downflow streams in the vicinity of the pier may be observed on water level variations.

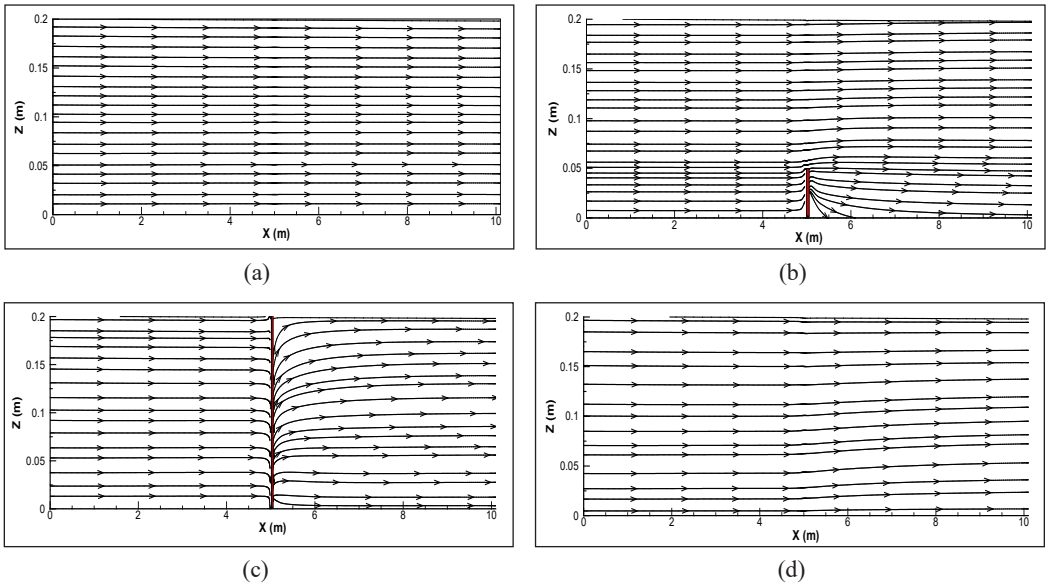

Figure 9. An instance of streamlines at longitudinal section at mid-channel in a) Test 1, b) Test 2, c) Test 3, and d) Test 4

Streamlines in Plan Views. To observe the influence of the piers in the channel, the study of the streamlines in plan is highly critical. As the magnifications of streamlines near the water surface in Figure 10 demonstrate, due to submergence of the damaged pier, no

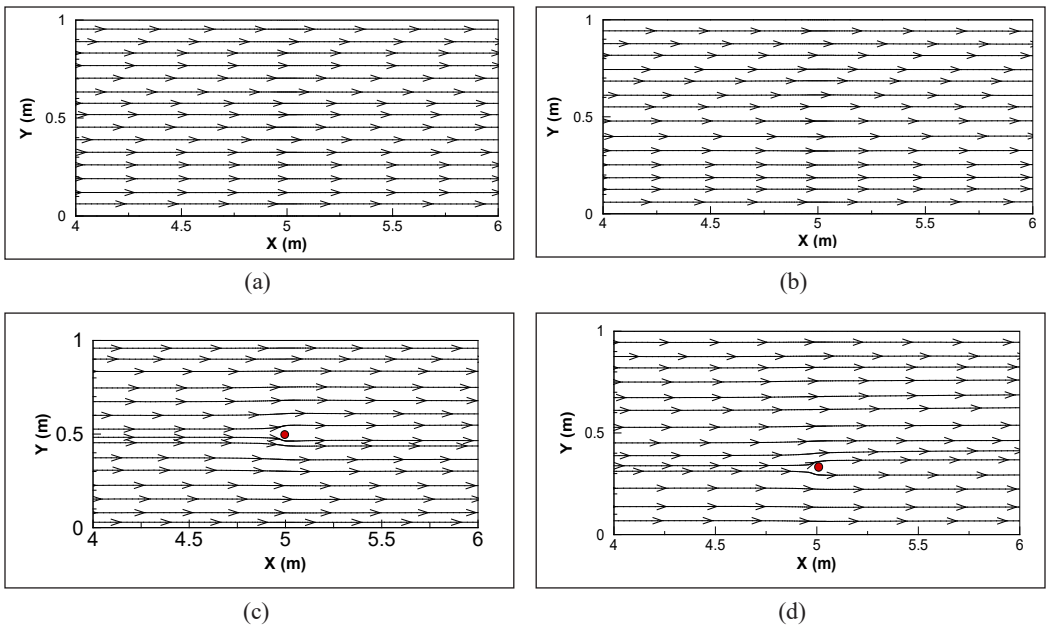

Figure 10. An instance of streamlines near the water surface in a) Test 1, b) Test 2, c) Test 3, and d) Test 4

significant effects have been observed in streamline variations at the water surface compared to the case with no piers installed. Although the streamline density due to presence of the pier is observable, the streamline variations are more significant where the intact pier is installed. Alteration and collision of the flow with the pier and increase in its density where both piers are installed are the combined effects resulting in velocity increase in this case.

Water Level Variations

Water level variations along the channel have been depicted in Figure 11 in different cases in the presence or absence of piers. As is observed in this figure, the water level is significantly influenced by presence of the intact pier, and its variations compared to the

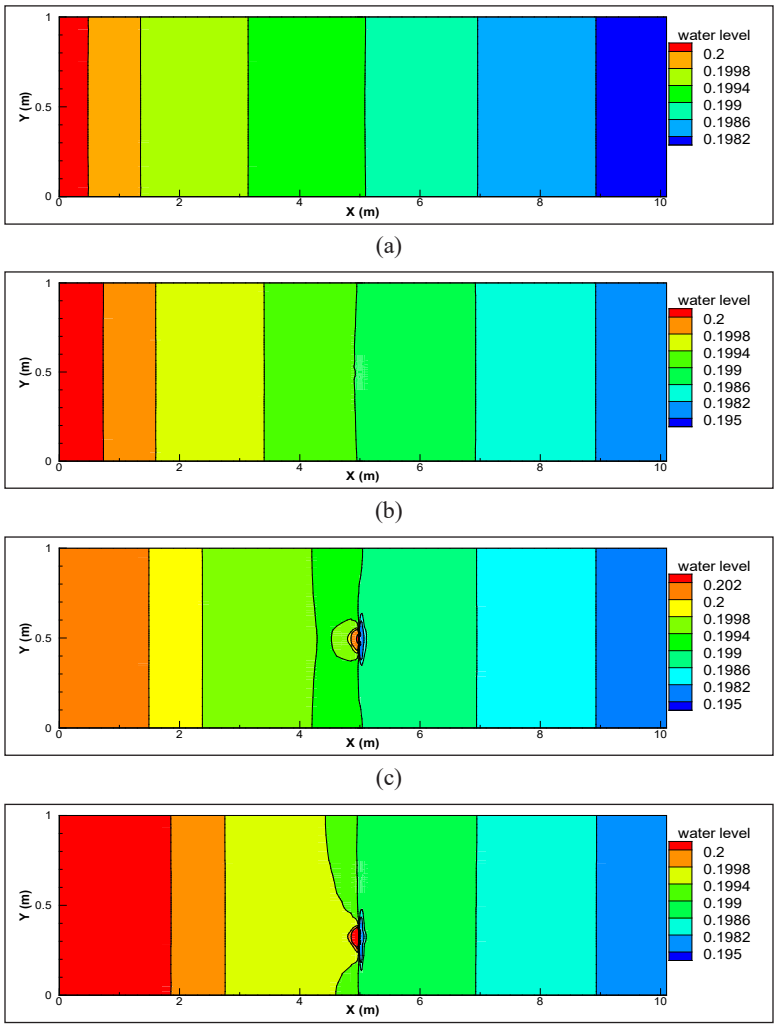

Figure 11. Water level variations in a) Test 1, b) Test 2, c) Test 3, and d) Test 4

installation of the damaged pier are evident. According to this figure, the water level is lowered at the downstream side of the intact pier due to the presence of downflow streams, and it is raised at the upstream side due to presence of upflow streams. However, this is intensified with installation of both piers so that it influences a wider range at mid-channel.

Bed Shear Stress Variations

Shear stress is a parameter of high significance. Through knowledge of this parameter, assessment of scouring or sedimentation at different points of bed is made viable (Abdi Chooplou & Vaghefi, 2019). Therefore, Figure 12 illustrates bed shear stress variations in

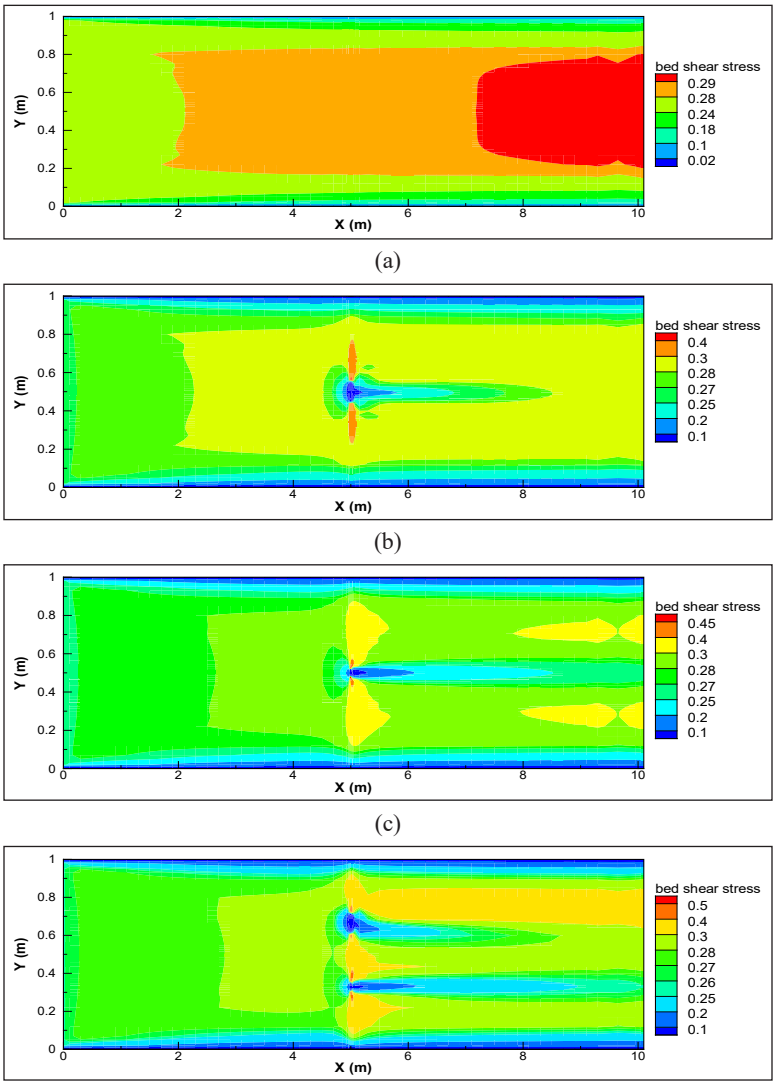

Figure 12. Bed shear stress variations in a) Test 1, b) Test 2, c) Test 3, and d) Test 4

different cases. Variations in position and the maximum value of bed shear stress affected by installation of the pier may be observed in this figure. As seen in Figure 12, installation of the piers has moved the maximum bed shear stress from the last one-third of the channel to mid-channel, in the vicinity of the piers. It is also observed that in the vicinity of the piers, the areas demonstrate less stress as a result of the present tranquil flow; however, at the upstream and downstream sides of the piers, the maximum stress occurs. Therefore, a 72% increase in the maximum bed shear stress occurs in the case of both piers installed as compared to the case with no piers.

CONCLUSIONS

This study has examined the flow pattern around intact and damaged bridge piers using experimental and numerical methods. To this aim, ADV and PIV had been utilized to conduct flow pattern experiments. Also, SSIIM was the numerical model used in this study. A summary of the most important conclusions obtained from this work is indicated below:

- A comparison between ADV and SSIIM data indicates the validity of the numerical model data and capability of this software to simulate the flow pattern around intact and damaged bridge piers.
- The maximum difference between numerical and experimental data is at layers near the bed; however, the total average of the errors in all four cases is 5% and acceptable.
- The difference between the average flow longitudinal velocities collected using ADV and PIV has been approximately 4%, which is negligible.
- The combined effect of damaged and intact piers creates downflow streams in the area of the piers.
- A tranquil and semi-stagnant area has been formed between the two piers due to the creation of low-velocity streams.
- The maximum water level variations occur in the case with both intact and damaged piers installed due to presence of upflow and downflow streams at the downstream and upstream sides of the piers.
- Installation of damaged and intact piers has moved the position of the maximum bed shear stress from the last one-third of the channel to mid-channel.
- The maximum bed shear stress has increased by 72% in comparison to the case with no piers installed.

ACKNOWLEDGEMENT

The authors of the paper would like to extend their most sincere appreciation to Islamic Azad University of Kerman branch for their cooperation in construction and installation of the flume.

REFERENCES

Abdi Chooplou, C., & Vaghefi, M. (2019). Experimental study of the effect of displacement of vanes submerged at channel width on distribution of velocity and shear stress in a 180 degree bend. *Journal of Applied Fluid Mechanics*, *12*(5), 1417-1428.

Akbari, M., & Vaghefi, M. (2017). Experimental investigation on streamlines in a 180º sharp bend. *Acta Scientiarum Technology*, *39*(4), 425-432.

Asadollahi, M., Vaghefi, M., & Tabib Nazhad Motlagh, M. J. (2019). Experimental and numerical comparison of flow and scour patterns around a single and triple bridge piers located at a sharp 180 degrees bend. *Scientia Iranica*, *2019*, 1-46.

Khajeh, S. B. M., Vaghefi, M., & Mahmoudi, A. (2017). The scour pattern around an inclined cylindrical pier in a sharp 180-degree bend: an experimental study. *International Journal of River Basin Management*, *15*(2), 207-218.

Bozkus, Z., & Cesme, M. (2010). Reduction of scouring depth by using inclined piers. *Canadian Journal of Civil Engineering*, *37*(12), 1621-1630.

Bozkus, Z., & Yildiz, O. (2001, August 27-31). Experimental investigation of scouring around inclined bridge piers. In *Proceedings of Wetlands Engineering and River Restoration* (pp. 1-12). Reno, Nevada.

Bozkuş, Z., Özalp, M. C., & Dinçer, A. E. (2018). Effect of pier inclination angle on local scour depth around bridge pier groups. *Arabian Journal for Science and Engineering*, *43*(10), 5413-5421.

Breusers, H. N. C., & Raudkivi, A. J. (1991). *Scouring hydraulic structures design manual*. Rotterdam, Netherlands: IAHR, AA Balkema.

Chiew, Y. M., & Melville, B. W. (1987). Local scour around bridge piers. *Journal of Hydraulic Research*, *25*(1), 15-26.

Chiew, Y. M., & Melville, B. W. (1996, June 22-28). Temporal development of local scour depth at bridge piers. In *Proceedings of North American Water and Environment Congress* (pp. 59-65). Anaheim, California, USA.

Duncan, J., Dabiri, D., Hove, J., & Gharib, M. (2011). Universal outlier detection for particle image velocimetry (PIV) and particle tracking velocimetry (PTV) data. *Measurement Science and Technology*, *21*(5), 1-5.

Goring, D. G., & Nikora, V. I. (2002). Despiking acoustic doppler velocimeter data. *Journal of Hydraulic Engineering*, *128*(1), 117-126.

Hurther, D., & Lemmin, U. (2001). A correction method for turbulence measurements with a 3D acoustic Doppler velocity profiler. *Journal of Atmospheric and Oceanic Technology*, *18*(3), 446-458.

Islam, M. R., & Zhu, D. Z. (2013). Kernel density–based algorithm for despiking ADV data. *Journal of Hydraulic Engineering*, *139*(7), 785-793.

Jaman, H., Das, S., Kuila, A., & Mazumdar, A. (2017). Hydrodynamic flow patterns around three inline eccentrically arranged circular piers. *Arabian Journal for Science and Engineering, 42*(9), 3973-3990.

Kara, S., Stoesser, T., & Sturm, T. W. (2012). Turbulence statistics in compound channels with deep and shallow overbank flows. *Journal of Hydraulic Research*, *50*(5), 482-493.

Karimi, N., Heidarnejad, M., & Masjedi, A. (2017). Scour depth at inclined bridge piers along a straight path: A laboratory study. *Engineering Science and Technology, an International Journal*, *20*(4), 1302-1307.

Lemmin, U., & Rolland, T. (1997). Acoustic velocity profiler for laboratory and field studies. *Journal of Hydraulic Engineering*, *123*(12), 1089-1098.

Melville, B. W., & Coleman, S. E. (2000). *Bridge scour*. Colorado, USA: Water Resources Publication.

Mori, N., Suzuki, T., & Kakuno, S. (2007). Noise of acoustic Doppler velocimeter data in bubbly flows. *Journal of Engineering Mechanics*, *133*(1), 122-125.

Nabipour, M., Neyshabouri, A. A. S., Dodaran, R. S., Zarrati, A. R., Mohajeri, H., & Zabetian, M. (2018). Experimental study of side looking ADV probe accuracy in a turbulent flow field. *Journal of Mechanical Engineering, 18*, 406-412.

Nezu, I., & Nakagawa, H. (1993). *Turbulence in open channel flows*. Rotterdam, Netherlands: IAHR, AA Balkema.

Nortek, A. S. (2009). *Vectrino velocimeter user guide*. Vangkroken, Norway: Nortek AS.

Olsen, N. R. B. (1999). *Computational fluid dynamics in hydraulic and sedimentation engineering*. Trondheim, Norway: The Norwegian University of Science and Technology.

Olsen, N. R. B. (2001). *CFD modeling for hydraulic structures*. Trondheim, Norway: The Norwegian University of Science and Technology.

Olsen, N. R. B. (2003). Three-dimensional CFD modeling of self-forming meandering channel. *Journal of Hydraulic Engineering*, *129*(5), 366-372.

Omara, H., Elsayed, S. M., Abdeelaal, G. M., Abd-Elhamid, A. F., & Tawfik, A. (2018). Hydromorphological numerical model of the local scour process around bridge piers. *Arabian Journal for Science and Engineering*, *44*(5), 4183-4199.

Raffel, M., Willert, C. E., Scarano, F., Kähler, C. J., Wereley, S. T., & Kompenhans, J. (2018). *Particle image velocimetry: a practical guide*. Berlin, Germany: Springer.

Raudkivi, A. J., & Ettema, R. (1983). Clear-water scour at cylindrical piers. *Journal of Hydraulic Engineering*, *109*(3), 338-350.

Razaz, M., & Kawanisi, K. (2011). Signal post-processing for acoustic velocimeters: Detecting and replacing spikes. *Measurement Science and Technology*, *22*(12), 1-11.

Razaz, M., Kawanisi, K., Nistor, I., & Sharifi, S. (2013). An acoustic travel time method for continuous velocity monitoring in shallow tidal streams. *Water Resources Research*, *49*(8), 4885-4899.

Rusello, P., Lohrmann, A., Siegel, E., & Maddux, T. (2006, September 10-13). Improvements in acoustic Doppler velocimetry. In *Proceedings of 7th International Conference on Hydroscience and Engineering* (pp. 1-16). Philadelphia, USA.

Schlichting, H. (1979). *Boundary layer theory.* New York, USA: McGraw-Hill.

Shinneeb, A. M., Bugg, J. D., & Balachandar, R. (2004). Variable threshold outlier identification in PIV data. *Measurement Science and Technology*, *15*(9), 1722-1732.

Thielicke, W., & Stamhuis, E. J. (2014). PIVlab-towards user-friendly, affordable and accurate digital particle image velocimetry in MATLAB. *Journal of Open Research Software*, *2*(1), 1-30.

Tominaga, A., & Nezu, I. (1991). Turbulent structure in compound open-channel flows. *Journal of Hydraulic Engineering*, *117*(1), 21-41.

Vaghefi, M., & Akbari, M. (2019). A procedure for setting up 180-degree sharp bend flume including construction and examinations with hydraulic structures. *Scientia Iranica*, *26*(6), 103-121.

Vaghefi, M., Alavinezhad, M., & Akbari, M. (2016a). The effect of submergence ratio on flow pattern around short T-head spur dike in a mild bend with rigid bed using numerical model. *Journal of the Chinese Institute of Engineers*, *39* (6), 666-674.

Vaghefi, M., Ghodsian, M., & Salimi, S. (2016b). The effect of circular bridge piers with different inclination angles toward downstream on scour. *Sadhana*, *41*(1), 75-86.

Vaghefi, M., Safarpoor, Y., & Akbari, M. (2016c). Numerical investigation of flow pattern and components of three-dimensional velocity around a submerged T-shaped spur dike in a 90° bend. *Journal of Central South University*, *23*(11), 2984-2998.

Vaghefi, M., Safarpoor, Y., & Akbari, M. (2017). Numerical comparison of the parameters influencing the turbulent flow using a T-shaped spur dike in a 90° bend. *Journal of Applied Fluid Mechanics*, *10*(1), 231-241.

Vaghefi, M., Faraji, B., Akbari, M., & Eghbalzadeh, A. (2018a). Numerical investigation of flow pattern around a T-shaped spur dike in the vicinity of attractive and repelling protective structures. *Journal of the Brazilian Society of Mechanical Sciences and Engineering*, *40*(2), 93-108.

Vaghefi, M., Tabibnezhad, M. J., Hashemi, S. S., & Moradi, S. (2018b). Experimental study of bed topography variations due to placement of a triad series of vertical piers at different positions in a 180° bend. *Arabian Journal of Geosciences*, *11*(5), 102-115.

Vaghefi, M., Mahmoodi, K., & Akbari, M. (2019a). Detection of outlier in 3D flow velocity collection in an open-channel bend using various data mining techniques. *Iranian Journal of Science and Technology, Transactions of Civil Engineering*, *43*(2), 197-214.

Vaghefi, M., Mahmoodi, K., & Akbari, M. (2019b). Application of artificial neural networks to predict flow velocity in a 180 degree sharp bend with and without a spur dike. *Soft Computing*, *2019*, 1-17.

Vaghefi, M., Radan, P., & Akbari, M. (2019c). Flow pattern around attractive, vertical, and repelling T-shaped spur dikes in a mild bend using CFD Modeling. *International Journal of Civil Engineering*, *17*(5), 607-617.

Voulgaris, G., & Trowbridge, J. H. (1998). Evaluation of the acoustic Doppler velocimeter (ADV) for turbulence measurements. *Journal of Atmospheric and Oceanic Technology*, *15*(1), 272-289.

Westerweel, J., & Scarano, F. (2005). Universal outlier detection for PIV data. *Experiments in Fluids*, *39*(6), 1096-1100.

Yafei, H. (2015). Discussion on the development of algorithm for despiking ADV data. *International Journal of Science and Research*, *4*(8), 1018-1020.

Yeow, S. C., Chanson, H., & Wang, H. (2016). Impact of a large cylindrical roughness on tidal bore propagation. *Canadian Journal of Civil Engineering*, *43*(8), 724-734.